

Received 22 July 2024, accepted 11 August 2024, date of publication 10 September 2024, date of current version 20 September 2024.

Digital Object Identifier 10.1109/ACCESS.2024.3455255



Prediction of State-of-Health and Remaining-Useful-Life of Battery Based on Hybrid Neural Network Model

LE THI MINH LIEN¹, VU QUOC ANH¹⁰, NGUYEN DUC TUYEN¹⁰, (Senior Member, IEEE), AND GORO FUJITA², (Member, IEEE)

¹Power Grid and Renewable Energy Laboratory, Department of Electrical Engineering, School of Electrical and Electronic Engineering, Hanoi University of Science and Technology, Hanoi 11615, Vietnam

²Department of Electrical Engineering, College of Engineering, Shibaura Institute of Technology, Tokyo 135-8548, Japan

Corresponding author: Nguyen Duc Tuyen (tuyen.nguyenduc@hust.edu.vn)

ABSTRACT Battery energy storage systems, especially lithium-ion batteries, have become more common in power systems owing to their numerous advantages, such as supporting voltage and frequency regulation and contributing to peak shaving and load shifting. However, when the battery reaches its end-of-life, it becomes more unstable, leading to a higher probability of system operation failure and safety accidents. Therefore, to accurately predict the State of Health (SOH) and the Remaining Useful Life (RUL) of a battery system, a prediction method is proposed in this paper based on Empirical Mode Decomposition (EMD), Bidirectional Long Short-Term Memory (BiLSTM), Convolutional Neural Network (CNN), and Attention Mechanism (AM). Firstly, capacity and different health indicators with high correlation extracted from the battery's charging and discharging characteristics are considered inputs. Then, the EMD method decomposes the battery data into several intrinsic mode functions (IMFs) and a residual. In the second part, with IMFs and a residual as input parameters, the SOH and RUL of different battery datasets are predicted by using the combined model CNN-BiLSTM-AM. To validate the accuracy of the proposed method, different comparative models are considered and carried out on CALCE and NASA battery degradation datasets. The results illustrate that the errors of the proposed method, which are root mean square error and mean absolute error are at least 48% and 19% more accurate than others in all battery datasets, showing the effectiveness and accuracy of the proposed model in predicting the SOH and RUL of the battery.

INDEX TERMS State of health, remaining useful life, health indicator, correlation coefficient, convolutional neural network, bidirectional long short-term memory, attention mechanism.

I. INTRODUCTION

Lithium-ion (Li-ion) batteries, with notable characteristics such as a larger storage capacity, higher durability, and lower discharge rate than traditional lead-acid batteries, have been widely applied in various industrial domains [1]. Nevertheless, degradation is a crucial and challenging problem for expanding the utilization of Li-ion batteries. In practice, the performance of batteries will gradually degrade with

The associate editor coordinating the review of this manuscript and approving it for publication was Yifan Zhou.

repeated charge/discharge cycles or deteriorate severely due to unexpected risks [2]. In the industry, battery degradation is determined through time, and charging/discharging cycles are regarded, especially with the high penetration of renewable energy into the power system. Therefore, accurate Li-ion batteries' health condition forecasting is imperative to ensure the operation of batteries with high reliability. The State of Health (SOH) and Remaining useful life (RUL) are two significant indicators of the battery health diagnosis system. SOH defines the battery aging level, and RUL represents the remaining period before the battery's useful



life ends. To date, SOH estimation methods are classified into three main categories: direct measurement, model-based, and data-driven.

Direct measurement approaches are based on direct computations, such as open-circuit voltage for capacity or Electrochemical Impedance Spectroscopy for impedance [3], [4]. Although this approach has low computational complexity and obtains accurate SOH, it is time-consuming and may not capture subtle changes or degradation trends over time.

In model-based methods, mathematical relations are built to represent the physical properties, thus fitting the degradation curve of a battery. Numerous models with priority knowledge of batteries have been employed for SOH and RUL prediction, for example, the Kalman Filtering (KF) method [5], Extended KF (EKF) [6], adaptive EKF [7], and Particle Filtering methods [8]. In general, modelbased approaches require a significant amount of expert knowledge along with a large volume of calculations. However, several existing drawbacks of these methods render them less prevalent in the area of SOH and RUL forecast, such as Implementing a model with accurate parameters in every cycle is challenging due to complicated internal electrochemical characteristics, or the forecast accuracy of filtering methods might be affected negatively due to particle impoverishment problem.

Data-driven methods without the requirements for battery degradation mechanisms have been increasingly adopted in this field. The data-driven method, perceived as a "black box" due to its incomprehensible internal workings, uses historically measured data of variables in the charging/discharging cycle such as voltage, cycle, and charge/discharge current. Recently, various intelligent algorithms such as Linear Regression (LR) [9], Gaussian Procession Model (GPM) [10], and Support Vector Machine (SVM) [11] have been applied to battery health prediction. In [12], a SOH and RUL prediction was proposed using the GPM considering Indirect Heath Indicators. Vilsen et al. [13] proposed a Multiple LR (MLR) for reducing the number of features, increasing the efficiency in SOH prediction. Lin et al. [14] implemented a multi-feature-based multimodel fusion method for predicting the SOH of the lithiumion battery. Different models, including MLR, GPR, and Support Vector Regression, were used, increasing accuracy and robustness. However, these models struggle to capture temporal information from input data.

Currently, the research based on Neural Networks (NN) is augmenting both quantity and quality. For instance, a Recurrent Neural Network (RNN) constitutes a category of neural architectures adept at managing sequential or temporal data by maintaining a concealed state, which encapsulates pertinent information from antecedent temporal instances. Lu et al. [15] evolved a SOH and RUL prediction framework based on RNN, incorporating forthcoming current plans and a limited set of initial capacity-voltage data as input. However, RNN struggles with exploding and vanishing

gradient problems, leading to less accuracy in predicting the battery's health. Hence, several models developed from RNN are introduced, such as Gated Recurrent Unit (GRU) [16] and Long Short-Term Memory (LSTM) [17]. Ungurean et al. [18] proposed an online SOH prediction method based on the GRU model. The results illustrated the forecast accuracy of the technique, concurrently conducting a comparative analysis between GRU and LSTM, thereby illustrating the parity in predictive capabilities exhibited by both models. Ma et al. [11] implemented a model-based improved LSTM and Health Indicators (HIs) extraction to estimate the SOH of the battery. Differential evolution grey wolf optimizer is introduced in optimizing hyper-parameters, and the results indicated competence in accuracy, robustness, and generalization. In general, both LSTM and GRU are effective models for capturing temporal dependencies and handling time series data. GRU, despite being designed to reduce the computation of the LSTM model, is less effective in capturing long-term dependencies as well as handling complex temporal patterns. Moreover, for capturing bidirectional dependencies, a Bidirectional LSTM (BiLSTM) model combined from two LSTM layers with opposite directions is more suitable. In [19], an incremental energy analysis (IEA) and BiLSTM-based method for estimating the SOH of the battery was carried out. The IE was first extracted and its relationship with the battery degradation was evaluated, then BiLSTM was utilized to capture the underlying mapping relationship between peak characteristics and SOH, resulting in the development of a battery SOH estimation model. The proposed model outperformed other compared models, which can be expressed through significantly smaller RMSE and higher R^2 .

However, these NN models are not appropriate to handle spatial patterns in data. Therefore, a Convolutional Neural Network (CNN) shows up as a solution to capture spatial patterns and short-term dependencies in time series data. The combination of the two models CNN and BiLSTM (or LSTM) provided an effective solution in capturing both long-term and short-term dependencies, both spatial and temporal patterns. The combination of suitable forecasting models, a practice that researchers have been employing, leads to more accurate time series data predictions by leveraging the strengths of the individual component models. Moreover, mastering long-term dependencies remains a substantial challenge, attributed to their restricted scalability in modeling extended sequences and the time-intensive nature of the training process. Hence, the Attention Mechanism (AM) is suggested to augment the model's capacity for capturing temporal dependencies while preserving interpretability [20], [21]. Self-attention Mechanism (SM) is also a mechanism enabling the model to focus on different parts of the input sequence with higher efficiency and flexibility. However, the SM is the core component of Transformer architectures, while AM better aligns with the architecture of BiLSTM. Moreover, AM's integration within the BiLSTM framework



allows for efficient handling of long-term dependencies without the extensive computational resources required by SM. Wang et al. [22] proposed a hybrid model including BiLSTM and AM models for SOH and RUL prediction. This paper used AM to extract features from the entire sequence by employing a weighted sum of all preceding input sequence states. Six Li-ion batteries were carried out, and the results indicated the predictive performance of the proposed method, which was revealed through several evaluation metrics. In [23], a combination of the CNN and Transformer model was employed for SOH estimation based on the NASA dataset. In data preprocessing, the Pearson correlation coefficient and the principal correlation analysis were applied to select the highly related features and decrease the complexity in computation, respectively. The predicted results indicated the high accuracy and stability of the proposed method.

Although combining different NN models can enhance the accuracy of SOH and RUL prediction, the denoising method was not included, which can still enlarge the deviation in the results. Cheng et al. [24] decomposed the raw degradation data by applying Empirical Mode Decomposition (EMD). Backpropagation LSTM with two structures used these handled data to predict the RUL and SOH of the battery. A model based on EMD, grey relational analysis (GRA), and deep RNNs was developed for estimating the SOH and RUL of lithium-ion batteries by Chen et al. [25]. First, the EMD and GRA methods extracted the characteristics of time series data, and then, several deep RNNs were implemented for SOH and RUL prediction. The current research is enhanced by analyzing another battery degradation dataset, simultaneously combining the use of both capacity and HI for estimating the SOH and RUL of the battery, drawing on methodologies proposed by Minh et al. in 2023 [26].

Health indicators are the features that can be extracted in the charging and discharging processes of the batteries. In general, HIs can be classified into two categories: Direct HI and Indirect HI [27]. Direct HIs refer to the capacity degradation and the increase in internal resistance of the battery, while indirect HIs relate to the features with high correlations with battery degradation. In paper [28], two HIs are extracted while the SOH is analyzed by applying the EMD method to decompose into IMFs and RES. In summary, the EMD-VCR-GRU-RF model is employed to estimate the SOH, improving both accuracy and computational efficiency. Liu et al. [29] proposed a SOH estimation method based on multi-feature extraction with a temporal convolution network. By combining Class I features extracted from charging and discharging curves with Class II features derived from EMD of battery capacity decay curves, the proposed model achieves enhanced SOH estimation accuracy.

Therefore, this paper proposes a hybrid model including EMD, BiLSTM, CNN, and AM, leveraging the strengths of each model while addressing the constraints outlined in the preceding article. Additionally, the model utilizes both capacity and highly correlated HI as inputs, further enhancing

its predictive capabilities. The EMD model is initially used for extracting the data into IMFs and a residual, which can limit the errors caused by the noise if using the initial degradation data. The advantages of each model are utilized to increase the accuracy of SOH and RUL prediction of the batteries. Moreover, different commonly used models are compared to illustrate the effectiveness in predicting SOH and RUL. In this study, the main contributions are given below:

- Different batteries from two datasets, namely CALCE and NASA, are used in this work. In addition to batteries under normal conditions, the degradation data from the batteries operated under extreme conditions are also considered to diversify the data, leading to an overall assessment of this model.
- Several Health Indicators are extracted from the charging and discharging process of the battery to contribute to predicting the SOH and RUL of the battery. However, for batteries operating under harsh conditions, using HI for forecasting may not be appropriate because the transformation patterns of the HIs are not highly correlated with the degradation of SOH.
- Establishing a data-based SOH and RUL prediction method using EMD, CNN, BiLSTM, and AM. The initial data is decomposed using the EMD method, which can effectively decompose complex signals into signals of different frequencies. This data then becomes the input of the CNN, subsequently passing through the BiLSTM and AM models, thereby providing the SOH and RUL predictions of the battery. The technique takes advantage of each component model to give accurate prediction results.
- Investigation and comparison of the prediction performance of the proposed model is carried out in terms of different battery datasets and the percentage of training data. The proposed model appears to outperform other compared models in all scenarios with different proportions of training data across both battery datasets. The RMSE and MAE respectively decrease by at least 48% and 19% when applying the CALCE battery dataset, in some cases, the proposed model can determine precisely the RUL of the batteries.

The structure of the paper is as follows. Section II describes each part of the proposed method and presents the method in this paper. Section III demonstrates the data used in this paper as well as the errors for evaluation. Section IV shows the prediction results and validates the accuracy and robustness of the proposed method by using different datasets with different percentages of training data and comparing them with other methods. Section V concludes this article.

II. DATA AND HEALTH INDICATORS EXTRACTION A. SOH AND RUL CALCULATION

SOH is an indicator of health through the aging process of the battery. SOH is usually defined through the ratio between the battery capacity at the current capacity C_i and the initial



capacity of the battery C_0 as follows:

$$SOH = \frac{C_i}{C_0} \times 100 \tag{1}$$

Due to physical reactions, the chemistry inside the battery causes the capacity of the battery to decrease over time. When the SOH of the battery drops below 70%, the battery needs to be replaced to ensure efficiency and safety for the user [30].

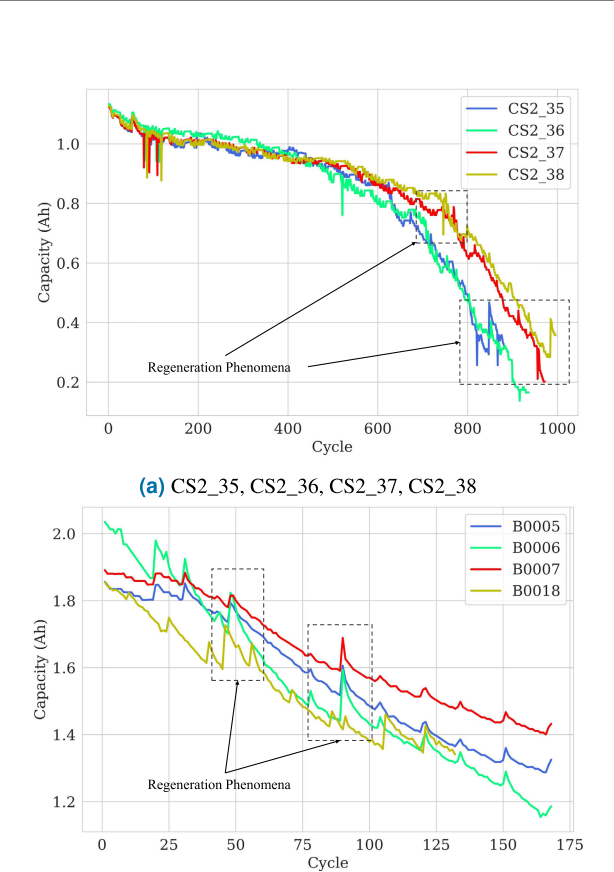
The battery's RUL index will indicate the battery's remaining number of applicable charge and discharge cycles. RUL is usually expressed by the difference between the total useful cycle of the battery before reaching a preset threshold and the cycle at the start of monitoring. The End of Monitoring (EOM) threshold is the initial capacity value utilized for RUL prediction, corresponding to the number of cycles T_{EOM} . When a battery's capacity falls below 70% of its standard value, it has reached its End of Life (EOL), corresponding to the number of cycles T_{EOL} . RUL is explicitly expressed through the formula below:

$$RUL = T_{EOL} - T_{EOM} \tag{2}$$

The battery's capacity will increase and decrease dramatically during the aging process because the battery has enough rest time for internal physical and chemical reactions to take place, carrying out the process of regenerating energy in the battery. This indicates that the battery's state changes frequently, demonstrating instability and nonlinearity. Therefore, accurate RUL prediction is necessary to solve more significant problems.

B. DATA

To determine the effectiveness of the proposed model, this paper uses two experimental datasets from the Center for Advanced Life Cycle Engineering (CALCE) at the University of Maryland [31] and the National Aeronautics and Space Administration (NASA)'s Prognostics Center of Excellence (PCoE) [32]. Data from CS2_35, CS2_36, CS2_37, and CS2_38 batteries from the CALCE dataset were selected for inclusion in the proposed model test. Those data are illustrated in Figure 1a. The CS2 batteries are all charged using a profile of constant current/ constant voltage (CC/CV), applying a CC charging mode with a charging rate of 0.5C until the voltage reaches a value of 4.2V. After that, the voltage value is maintained until the charging current drops below the value of 0.05A. In discharge mode, the cells are cycled at the CC of 1C, and the process will be stopped when the voltage reaches its cut-off value of 2.7V. These prismatic cells have a rated capacity of 1.1Ah and the minimal charge current is 50mA. The charging and discharging process of the batteries has been carried out at room temperature $(23^{\circ}C)$. Moreover, the End of Performance for these batteries is set at 0.85 Ah, hence, its EOL is about 77%. However, in this work, the EOL is set at 70%, which is about 0.77 Ah, since the battery's degradation is significant when its capacity decreases around 0.7 Ah as illustrated in Fig. 1a. Batteries CS2_35 and CS2_37 are chosen to carry out this research.



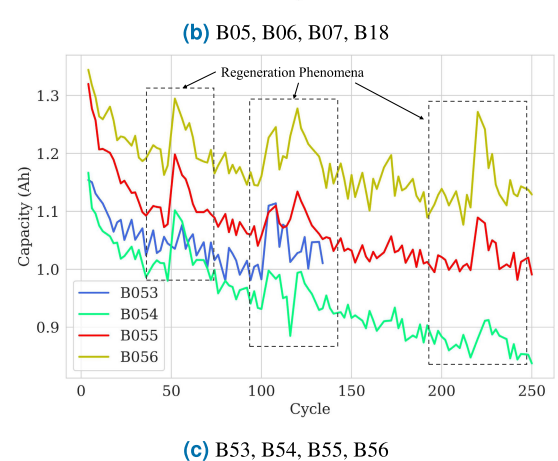


FIGURE 1. CALCE and NASA battery datasets.

On the other hand, NASA's 18650 lithium batteries with a rated capacity of 2Ah are run through different operating configurations (charging, discharging, impedance) at room temperature $(24^{o}C)$ for B05, B06, B07, and B18, or at an ambient temperature of $4^{o}C$, for B53 to B56. It is necessary to consider different batteries in different conditions, diversifying the data and making the validation more valuable. The battery's aging process is performed by repeated charging and discharging operations to accelerate the decline in battery capacity. Charging in the CC mode 1.5A is the charging process used mainly until the voltage reaches 4.2V, after which the batteries will continue to be charged in the constant voltage mode until the current

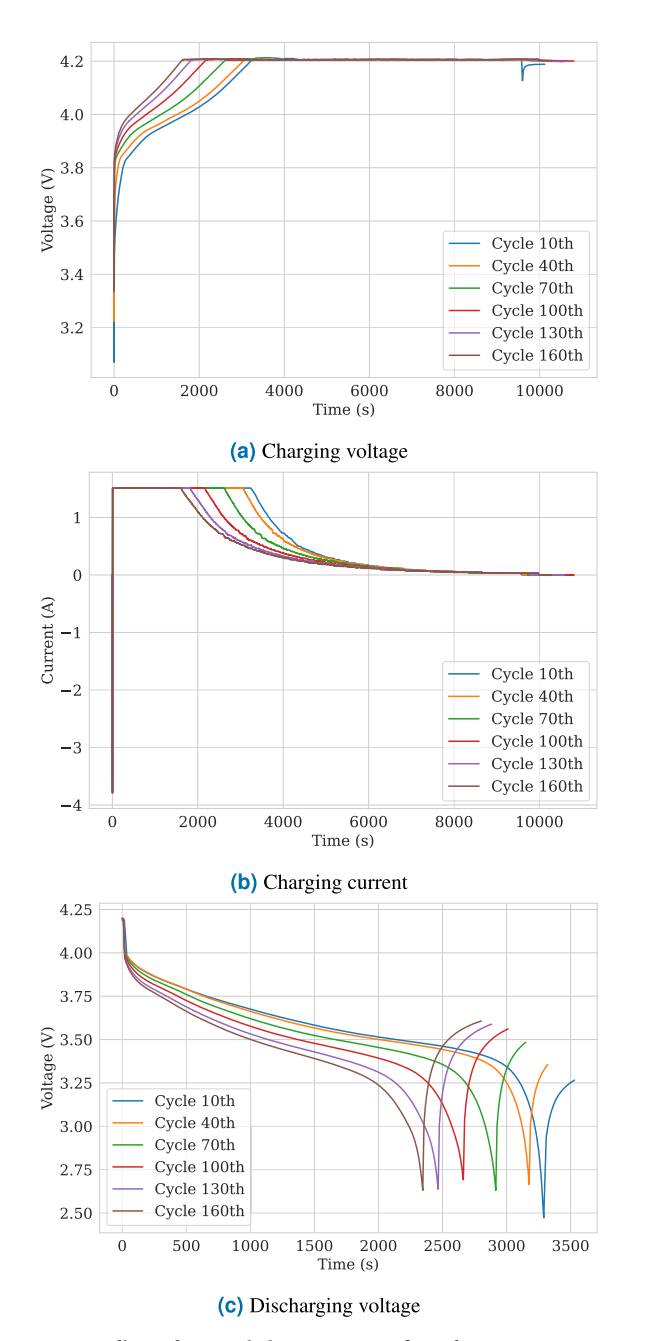


FIGURE 2. Indirect characteristic parameters of B05 battery.

drops to 20mA. The discharge of the batteries is carried out in the constant current mode of 2A. The discharge process will stop when reaching the cut-off voltages, which are 2.7V (B05, B56), 2.5V (B06, B18, B55), 2.2V (B07, B54), or 2V (B53). Moreover, the impedance was measured using electrochemical impedance spectroscopy (EIS) with a frequency sweep ranging from 0.1 Hz to 5 kHz. When 30% of the battery's capacity faded, the experiment stopped, hence the EOL of these batteries is set at 70%. The trend of capacity depletion of the batteries is shown in Figure 1c. In this work, B05, B06, B54 and B55 are selected. It is noted that the degradation of B54 and B55 batteries have significant fluctuations and harsh working conditions compared to other

chosen batteries, which is a substantial contribution to the assessment of the proposed model. The parameters of the two batteries dataset used in this paper are shown in Table 1. It should be noted that there are some increases in the capacity of the battery at several time intervals. This phenomenon is called regeneration, which occurs when the rest time lasts long enough [33]. The data used then be cleansed through a cleansing data process to wipe out most of the outliers, reducing their influence in predicting the SOH and RUL of the batteries.

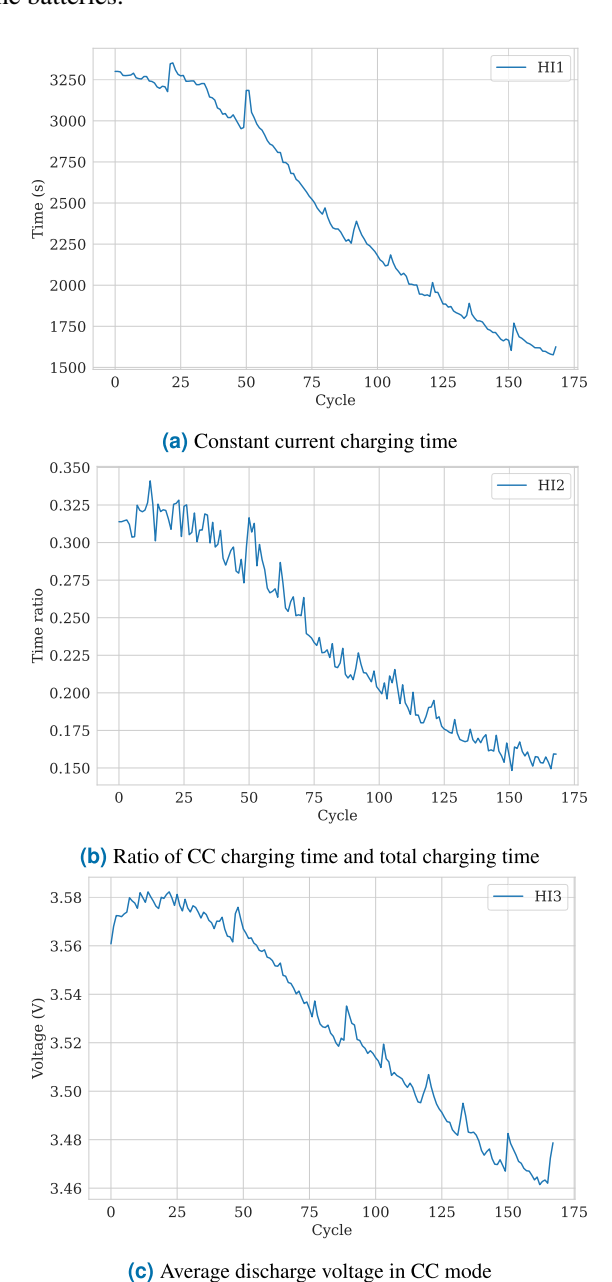


FIGURE 3. Health indicator results of B05 battery.

C. SELECTION OF HEALTH INDICATORS

In this part, different HIs are considered to determine through the charging and discharging processes, which indirectly



TABLE 1. Batteries degradation parameters.

Battery	CS2_35	CS2_37	B05	B06	B54	B55
Charging rate (C)	0.5	0.5	1.5	1.5	1.5	1.5
Maximum voltage (V)	4.2	4.2	4.2	4.2	4.2	4.2
Cut-off charging current (A)	0.05	0.05	0.02	0.02	0.02	0.02
Discharge rate (C)	1	1	2	2	2	2
Cut-off discharge voltage (V)	2.7	2.7	2.7	2.5	2.2	2.5
Rated capacity (Ah)	1.1	1.1	2	2	2	2
Working temperature (°C)	23	23	24	24	4	4
EOL (%)	70	70	70	70	70	70

reflect the SOH of the battery. Figure 2 illustrates the voltage and current of the B05 battery in both the charging and discharging phases. It can be seen from Figure 2b that when the cycle increases, or in other words, the capacity decays, the CC charging time decreases. This is due to the deepening of the battery polarization, leading to a decline in charging capacity. Therefore, two parameters named the CC charging time and the ratio between the CC charging time and the total charging time are selected as the health features for estimating the SOH and RUL of the battery. Moreover, in the battery discharging process, it is necessary to consider the average discharge voltage in CC mode. It's worth highlighting that while the battery's capacity can be determined by analyzing the discharging time in the CC mode, the average voltage calculated during that time interval will also exhibit specific correlations. The HIs extracted in this work can be seen in Figure 3. To verify the correlation between these HIs and the health of the battery, Pearson and Spearman correlation coefficients are utilized in this work. Pearson correlation measures the linear relationship between two continuous variables, while the Spearman correlation measures a monotonic relationship between two variables based on the rank of the data [34]. Pearson correlation and Spearman correlation coefficient can be calculated as follows:

$$p = \frac{\sum_{i=1}^{m} \left(HI_i - \overline{HI} \right) \left(SOH_i - \overline{SOH} \right)}{\sqrt{\sum_{i=1}^{m} \left(HI_i - \overline{HI} \right)^2 \sum_{i=1}^{m} \left(SOH_i - \overline{SOH} \right)^2}}$$
(3)

$$s = 1 - \frac{6\sum_{i=1}^{m} d_i^2}{m(m^2 - 1)} \tag{4}$$

where p and s are the Pearson and Spearman correlation coefficients, respectively, and d_i is the difference between the rank of HI and SOH. These correlation coefficients, ranging from -1 to 1, signify the strength and direction of the relationship between voltage and capacity. A higher absolute value closer to 1 indicates a stronger correlation,

providing valuable insights into the battery's health during charge and discharge cycles. The correlation results of all the battery datasets can be observed in Table 2. Both the Pearson correlations and the Spearman correlations of the HI are above 0.9, indicating a strong reflection of the battery degradation process. It is worth pointing out that B54 and B55 batteries have harsh working conditions, hence the change in the voltage and current when the capacity increases does not follow the rules as in the B05 or B06 battery. Therefore, for batteries with harsh operating conditions, directly using the capacity to predict will be more effective and accurate.

III. METHODOLOGY

The aim of employing multi-variable time series forecasting in this study is to anticipate the capacity output P_t by considering L observed values from the previous instances.

$$P_t = f(X^{N \times L}, P^L) \tag{5}$$

$$P_{t} = f(X^{N \times L}, P^{L})$$

$$\begin{cases} X^{N \times L} = (X_{t-L}^{N \times 1}, X_{t-L+1}^{N \times 1}, \dots, X_{t-1}^{N \times 1}) \\ P^{L} = (P_{T-L}, P_{T-L+1}, \dots, P_{T-1}) \end{cases}$$
(6)

where N denotes the number of dimensions in the dataset over the time span of $L; X^{N \times L}$, and P^{L} are the historical input data and output capacity data, respectively. The method proposed in this paper is a combination of the EMD, CNN, BiLSTM, and AM methods. The CNN-BiLSTM-AM model can predict the data in time series and be more accurate and robust by applying the EMD method in the data preprocessing section.

A. EMPIRICAL MODE DECOMPOSITION

EMD was initially introduced in [35] as an effective method for decomposing time-series data and interpreting their inherent properties. In the context of the battery's degradation data, the high-frequency signals correspond to the regeneration phenomena and local fluctuations, whereas the global trend can be characterized as low-frequency signals. EMD extracts time-series data into two elements: a series of intrinsic mode functions (IMFs) and a residual sequence based on an iterative process [36]. Each IMF stands for a particular frequency band extracted from the original data. The criteria for IMFs are as follows: First, for the entire dataset, the number of local extrema and zero-crossings of the differences between the original data and the average of the surrounding envelope differs at most by one; then, the average of the surrounding envelope equals to zero. EMD is considered an adaptive method since the number of IMFs correlates with the complexity of the data. The detailed procedure of EMD is shown below:

- 1) Compute extreme points indicated as the local minima i(t) and maxima a(t) of the original time series x(t)(Battery's capacity or SOH)
- 2) Connect these local extrema based on a cubic spline interpolation to implement the upper and lower envelopes

Battery	Health Indicators	Pearson coefficients	Spearman coefficients
	HI1	0.9957	0.9902
B05	HI2	0.9874	0.9764
	HI3	0.9925	0.9825
	HI1	0.9900	0.9904
B06	HI2	0.9857	0.9884
	HI3	0.9916	0.9957
	HI1	0.9887	0.9802
CS2_35	HI2	0.9222	0.9618
	HI3	0.9634	0.9328
	HI1	0.9931	0.9805
CS2_37	HI2	0.9128	0.9861
	HI3	0.9686	0.9349

TABLE 2. Pearson and spearman correlation results.

Calculate the mean of the surrounding envelope as follows:

$$m(t) = \frac{a(t) + i(t)}{2} \tag{7}$$

4) Compute the differences as the following equation:

$$d(t) = x(t) - m(t) \tag{8}$$

- 5) If the aforementioned stopping criteria are satisfied, then the first IMF = m(t) and the first residue R = d(t)
- 6) Repeat Steps 2-5 until *R* becomes a monotonic function. The iterative process will be terminated if the pre-defined number of iterations is reached.

B. CONVOLUTIONAL NEURAL NETWORK (CNN)

The CNN is a widely recognized deep learning framework by the natural visual perception mechanism observed in living beings [37]. Its precursor was first introduced in 1980 by Kunihiko Fukushima [38], and it was not until 1990 that CNN's modern framework was established by LeCun et al. [39]. The CNN model is commonly used for processing and extracting features from structured grid-like data. Unlike traditional neural networks, CNN, with specialized layers, is intended to capture spatial hierarchies and lessen the computing burden. A CNN architecture generally consists of 3 main parts: convolutional layer, pooling layer, and fully-connected layer [37]. Instead of using two-dimensional convolutional layers as in image data, this paper adopts one-dimensional CNN (1D-CNN) to extract local spatial features of time-series data [40]. About the procedure of the 1D-CNN model, the data is first set up and regulated in the input layer. Then, the convolutional layer uses filters, also called kernels, to slide over the input data to detect spatial hierarchies of features. The output feature map of the convolutional layer at the location i is calculated by:

$$H_{i} = ReLU(\sum_{j=1}^{M} X_{i+j-1} \times W_{co,j} + b_{co})$$
 (9)

where ReLU(.) denotes the Rectifier Linear Unit activation function, M is the size of the filter, X is the input sequence,

and W_{co} , and b_{co} are the weight and bias matrices, respectively. After that, the pooling layer reduces the temporal dimensional, decreasing the number of parameters. Max pooling is used in this paper, which selects the maximum value from a local input region due to feature retention and robustness improvement. The mathematical equation can be expressed as follows:

$$P_i = max\{H_{i,s}, H_{i,s+1}, \dots, H_{i,s+s-1}\}$$
 (10)

where P_i is the pooled value, and s is the pooling size. After the convolutional and pooling layer, the acquired features flatten into a single extended vector and traverse a fully connected layer or dense layer before reaching the output layer. Besides, the dropout is applied for overfitting prevention. The process can be interpreted by these equations:

$$F = [P_1, P_2, \dots, P_N] \tag{11}$$

$$Y = ReLU(W_f \times F + b_f) \tag{12}$$

where F is the flattened vector, Y is the output of the fully connected layer, and W_f , and b_f are the weight and bias matrices of the fully connected layer, respectively. The structure of the 1D-CNN network, in particular, and the basic CNN network, in general, can be indicated in Figure 4.

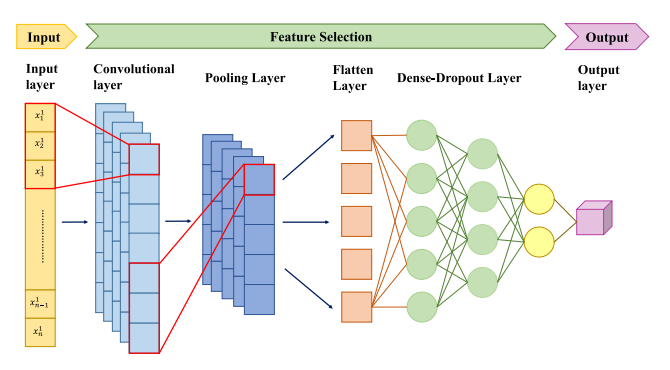


FIGURE 4. Structure of 1D-CNN network.

C. BIDIRECTIONAL LONG SHORT-TERM MEMORY (BILSTM)

LSTM was first introduced in 1997 [41], an advancement in the field of neural networks, particularly in comparison to



its predecessor, RNN. Unlike traditional RNNs, LSTM units include mechanisms such as input, forget, and output gates, allowing them to capture temporal dependencies better and handle time series data [42]. The operation of the LSTM cell is mathematically described as follows:

• Forget gate f_i : employs a sigmoid activation function to decide which parts of the current cell state should be retained and which should be forgotten.

$$f_t = \sigma \left(W_{fx} \times x_t + W_{fh} \times h_{t-1} + b_f \right) \tag{13}$$

where W_f and b_f denote the weight and bias matrices of the forget gate, x_t is the current input data, and h_{t-1} represents the previous hidden state.

Input gate i_t: operates by using a sigmoid activation function to decide which values from the input should be updated. Simultaneously, a tanh activation function produces a new candidate cell state C_t that could be added to the new cell state C_t.

$$i_t = \sigma \left(W_{ix} \times x_t + W_{ih} \times h_{t-1} + b_i \right) \tag{14}$$

$$\tilde{C}_t = \tanh\left(W_{cx} \times x_t + W_{ch} \times h_{t-1} + b_c\right) \tag{15}$$

$$C_t = f_t \times C_{t-1} + i_t \times \tilde{C}_t \tag{16}$$

where W_i , b_i , W_c , and b_c denote the weight and bias matrices of the input gate and memory cell, respectively, and C_{t-1} is the previous cell state.

 Output state o_t: controls the information outputted from the memory cell. The equation of o_t and the new hidden state h_t are as follows:

$$o_t = \sigma \left(W_{ox} \times x_t + W_{oh} \times h_{t-1} + b_o \right) \tag{17}$$

$$h_t = o_t * \tanh(C_t) \tag{18}$$

where W_o and b_o denote the weight and bias matrices of the output gate and * indicates the Hadamard product.

While LSTM is effective for tasks with unidirectional dependencies, BiLSTM offers a more comprehensive approach for capturing bidirectional dependencies. Therefore, BiLSTM is comprised of two LSTM layers with opposite directions, and the output h^\prime_t of the BiLSTM network is the result of a combination process expressed as follows:

$$h_f = LSTM\left(x_t, h_{f-1}\right) \tag{19}$$

$$h_b = LSTM(x_t, h_{b-1}) \tag{20}$$

$$h'_{t} = W_{hf} \times h_{f} + W_{hb} \times h_{b} + b_{h} \tag{21}$$

where h_f and h_b are the output of the forward and backward LSTM layer, respectively; W_{hf} and W_{hb} are the weight matrices corresponding to each layer, while b_h denotes the bias matrix. The visualization structure of a single LSTM cell and BiLSTM network can be illustrated in Figure 5 and Figure 6.

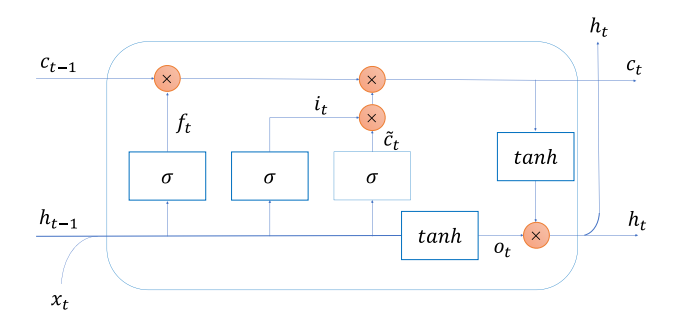


FIGURE 5. Structure of a single LSTM cell.

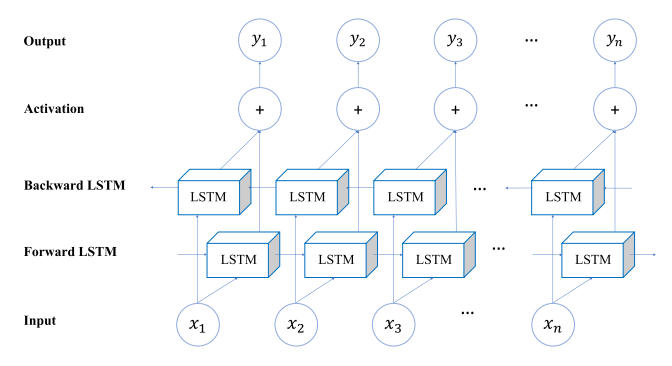


FIGURE 6. Structure of BiLSTM network.

D. ATTENTION MECHANISM

The AM draws inspiration from the way biological systems in humans concentrate on distinct components when handling extensive information. In deep learning, AM is a fundamental idea that allows models to focus on particular parts of input sequences selectively [43]. When applied to time series data, AM enables models to dynamically balance the importance of various temporal points, improving the models' capacity to represent long-range interdependence. Therefore, significant information is more focused on instead of unimportant details [44]. In this study, AM employs the hidden layer output vector of the BiLSTM network h'_t mentioned above as inputs, and then the AM will be mathematically described as follows:

• The correlation score e_{ij} between the i^{th} and j^{th} output $(h'_i \text{ and } h'_j)$ of the BiLSTM network is calculated as follows:

$$e_{ii} = f\left(W_i \times h'_i + W_i \times h'_i + b_{ii}\right) \tag{22}$$

where W_i and W_j are the weight matrices corresponding to h'_i and h'_j , respectively, and b_{ij} defines the bias matrix.

• Hereafter, the attention score α_{ij} will be computed based on the Softmax function and correlation score e_{ij} as the following equation:

$$\alpha_{ij} = \frac{\exp\left(e_{ij}\right)}{\sum\limits_{k=1}^{T} \exp\left(e_{ij}\right)'}, \sum a_{ij} = 1$$
 (23)



• Thereby, the output of the AM layer or the contribution of each input is calculated as follows:

$$H_k = \sum_j \alpha_{ij} \times h_j^{\,\prime} \tag{24}$$

The process of the AM model can be illustrated in Figure 7.

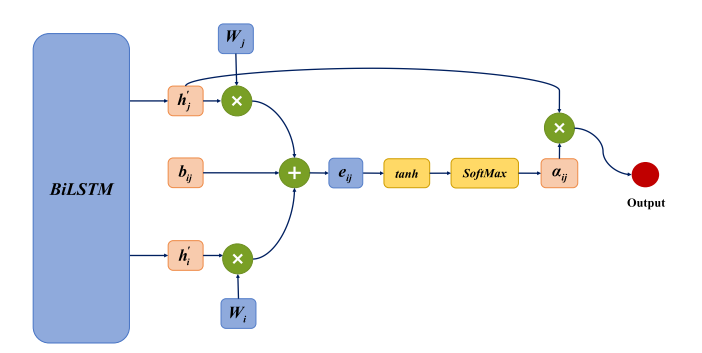


FIGURE 7. Structure of attention mechanism.

E. COMBINATION MODEL

Figure 8 indicates the detailed architecture of the combination model CNN-BiLSTM-AM (CBA). It should be noted that the raw data first went through the EMD, and the decomposed data, which are the IMFs, then became the input of the combination model. As can be observed from this figure, the model comprises three main components: CNN, BiLSTM, and AM. Detailed structure and operation of each one are presented in the previous sub-sections. The process to attain the output and forecast values is as follows: First, the 1D-CNN layer is adopted to extract global spatial features from the input sequences based on convolutional multiplication. Then, the output of the 1D-CNN layer is fed into the BiLSTM layer to obtain new vectors. To enhance the performance of the BiLSTM layer, these vectors are entered into the AM layer to be allocated weights effectively for each one based on the AM. After the weight distribution process finishes, the final value or the output is achieved. The overall process can be mathematically expressed as follows:

$$Y_{1} = ECBA(IMF_{1}, IMF_{2}, ..., IMF_{N})$$

$$= E(Con1D(BiLSTM(AM(IMF_{1}, IMF_{2}, ..., IMF_{N}))))$$
(25)

where Y_1 is the output of the CBA model, ECBA(.)denotes the EMD-CNN-BiLSTM-AM model, and E, Con1D, BiLSTM, and AM express the EMD, 1D-CNN, BiLSTM, and AM process, respectively.

The proposed framework for SOH estimation and RUL prediction in this study is represented in Figure 9. This framework is classified into three steps: data preprocessing, data processing, and data prediction. In the first step, the battery data is acquired, containing several parameters related to the battery module, such as capacity, SOH, and HIs. These parameters are decomposed into IMFs and RES using the EMD method. The detailed results of decomposition based on EMD are illustrated in the subsequent subsection. Hereafter, IMFs and RES are utilized as input variables entered into two separate forecasting models: CNN-BiLSTM-AM and LSTM. These deep learning models are described explicitly in the previous section. The second step processes the input to generate the predicted RUL and SOH. The output of the LSTM model using RES as the input and the overall process can be expressed as follows:

$$Y_2 = E(BiLSTM(RES)) \tag{26}$$

$$Y = Y_1 \oplus Y_2 \tag{27}$$

where Y_2 is the output of the LSTM model, and \oplus denotes the element-wise summation. In the last step, the performance of the proposed model is illustrated and evaluated based on three assessment metrics and validated by using several benchmark models for comparison.

IV. RESULTS AND DISCUSSION

A. EVALUATION METRICS

In this study, four performance criteria are adopted to assess the effectiveness of the proposed model in SOH estimation and RUL prediction. To evaluate the predictive performance of the proposed method, absolute error (AE), relative error (RE), root mean square error (RMSE), and mean absolute error (MAE) are used in this paper. They are defined as follows:

$$AE = \left| RUL_{pr} - RUL_{re} \right| \tag{28}$$

$$RE = \frac{|RUL_{pr} - RUL_{re}|}{RUL_{re}} \tag{29}$$

$$RE = \frac{\left|RUL_{pr} - RUL_{re}\right|}{RUL_{re}}$$

$$RMSE = \sqrt{\frac{1}{n} \sum_{t=1}^{n} (x_t - \hat{x}_t)^2}$$
(29)

$$MAE = \frac{1}{n} \sum_{t=1}^{n} \|x_t - \hat{x}_t\|$$
 (31)

where RUL_{pr} is the predicted RUL value, RUL_{re} is the actual RUL data, n is the cycle number, x_t is the actual capacity data, and \hat{x}_t is the predicted capacity data.

In this section, the battery data from two datasets, CALCE and NASA, is used to demonstrate the accuracy and robustness of the proposed method. The method compares the SOH and RUL predicted results with those of CNN-BiLSTM-AM, CNN-BiLSTM, and BiLSTM to verify the accuracy of the proposed method. In Section IV-B, the comparisons between methods are given using the CALCE dataset, and in Section IV-C, the NASA dataset is used to show the difference between those methods. In both sections, the SOH and RUL data results will be displayed. Different training rates are applied to show the changes when more data is employed to train.



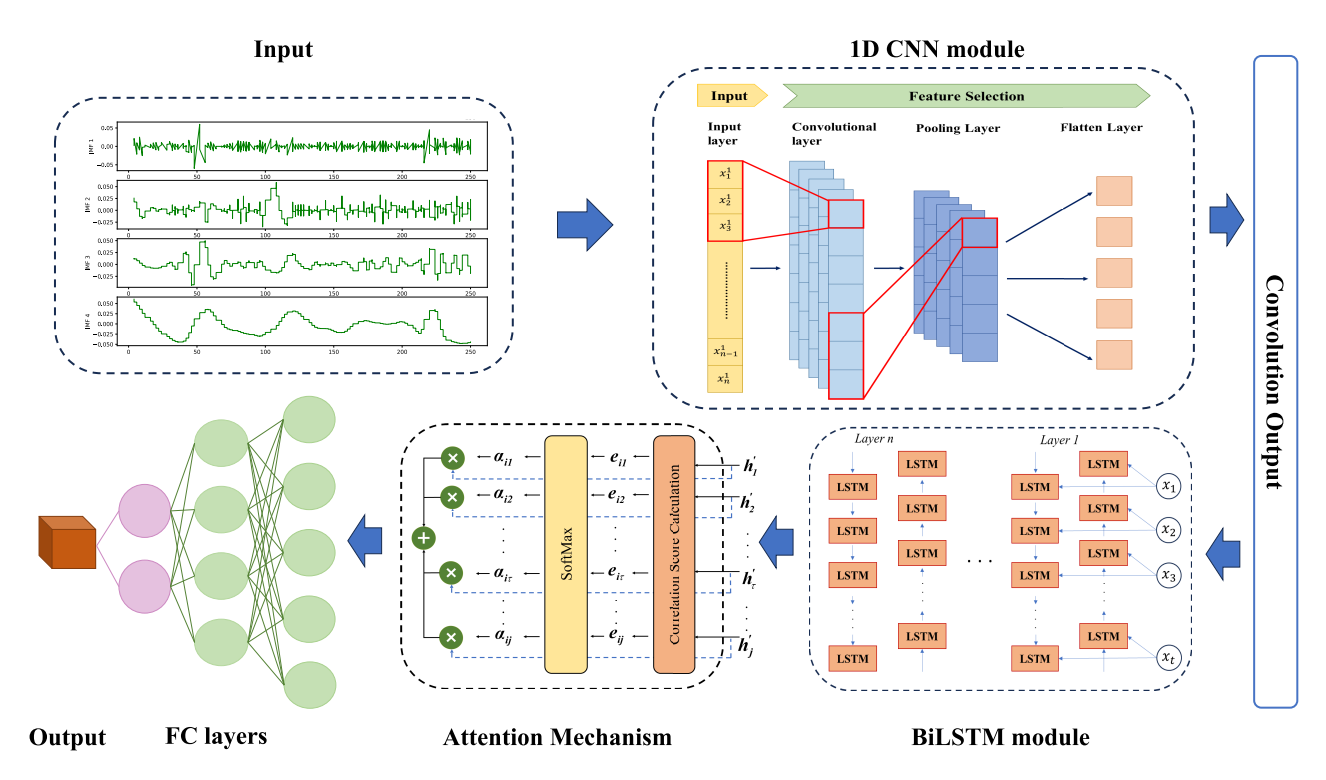


FIGURE 8. The architecture of the combination model (CNN-BiLSTM-AM).

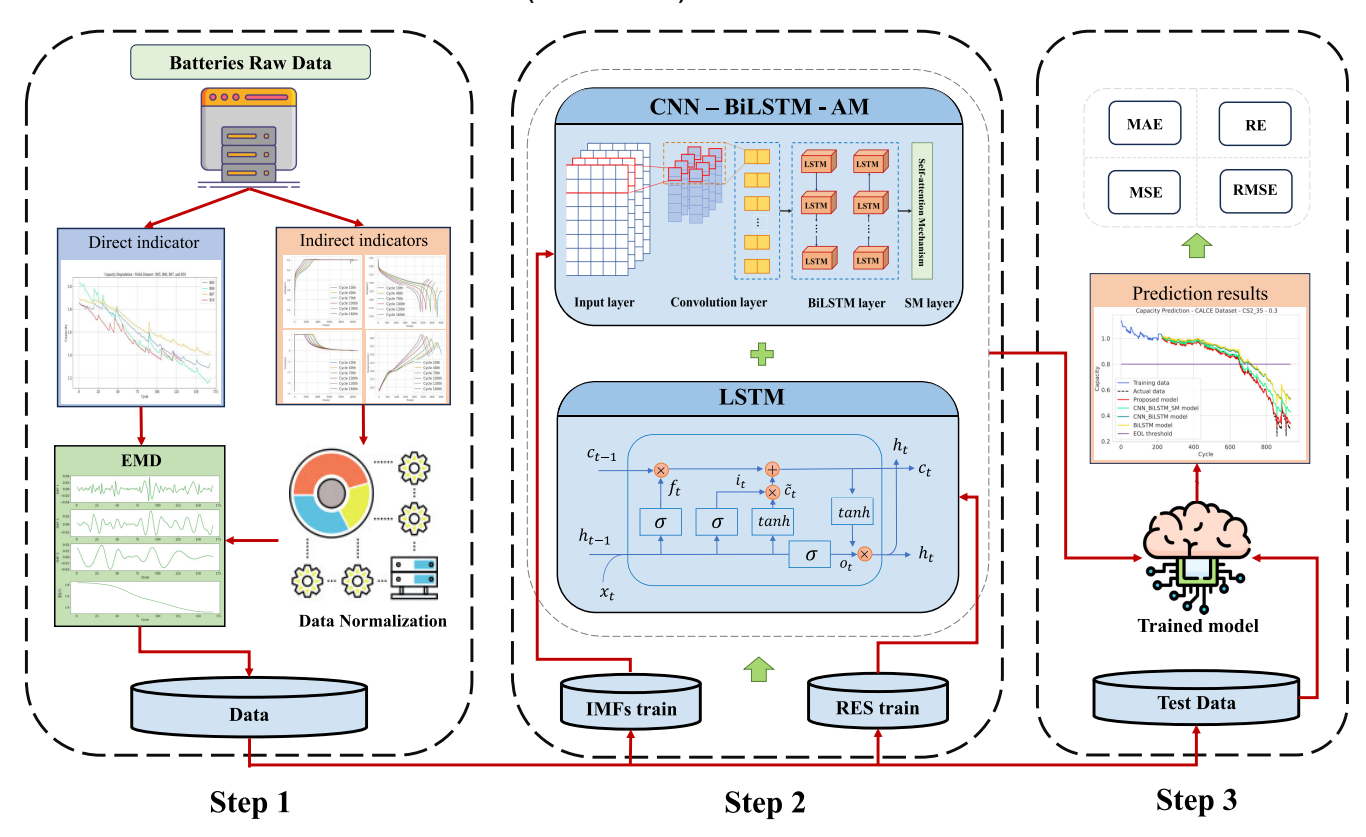


FIGURE 9. Proposed framework for SOH and RUL estimation.

B. EMD

In this paper, the EMD method is used to decompose the sequence data, including the capacity and several HIs, of the

battery into IMF sequences and a residual sequence. When applying CALCE battery datasets, two IMFs and a RES were extracted in each battery, as shown in Figure 10. In general,

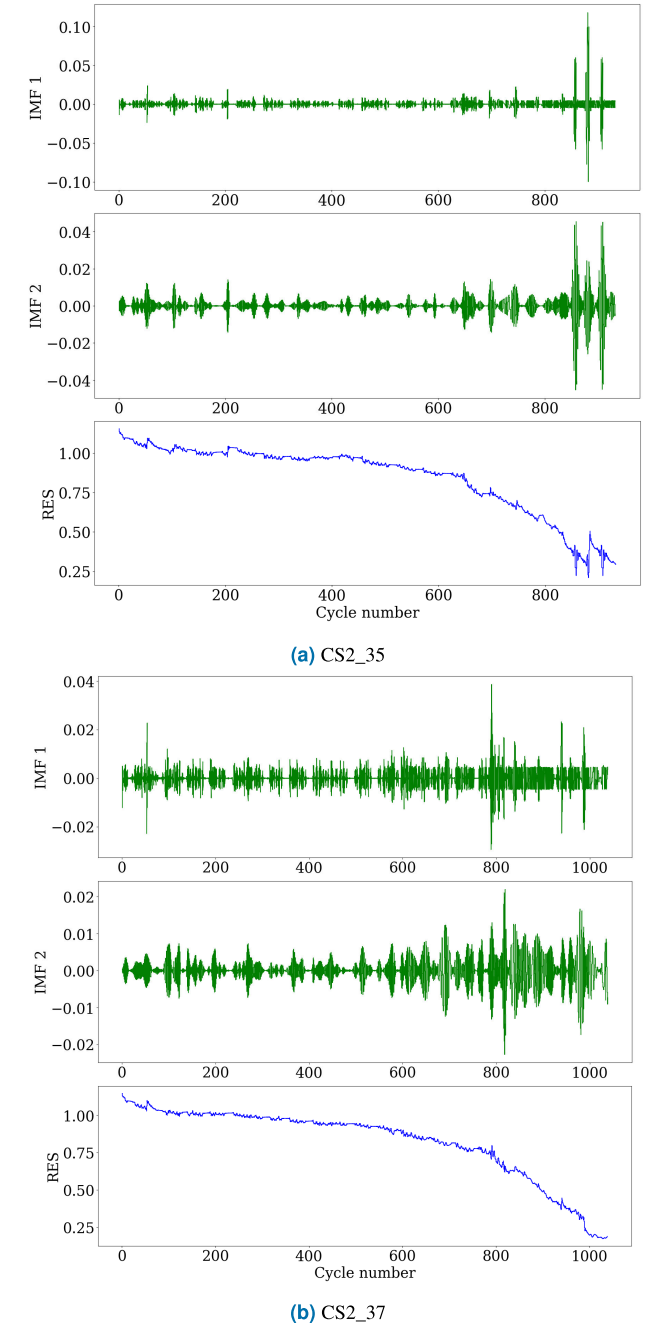


FIGURE 10. IMFs and RES data of CALCE datasets.

the local or high frequencies are removed by the EMD method and are captured by two IMF sequences. The remaining data after separation is obtained by residual, which presents the overall trend of the data. Due to the number of IMFs that have decomposed, RES cannot be obtained as a less fluctuating curve. In this case, the error will be cumulative if the amount of IMF sequences increases.

Figure 11a and Figure 11b illustrate the corresponding decomposition results of B05 and B06 batteries. For these two battery datasets, the local or high frequencies are removed by the EMD method, and each is captured by two IMF

sequences. The remaining data after separation is obtained by residual, which presents the overall trend of the data. There are similarities between the IMF sequences and the residual sequence. Similar to the CALCE battery datasets, there are only 2 IMFs extracted by using the EMD method due to the increase in error. However, for B54 and B55 batteries, four or five IMF sequences were decomposed from the source data instead of two, which can be illustrated in Figure 11c and Figure 11d. The increase in the number of IMFs is caused by the significant fluctuation of the two battery datasets, which relates to their harsh working conditions. In general, IMF1 possesses the most fluctuation; the variability gradually decreases, and by IMF4, its trend becomes softer. The residual sequences of these two battery datasets still present monotonous health trends. However, when extracting more IMF, the residuals of these two batteries are smoother than those of batteries B05 and B06.

C. CALCE BATTERY DATASET

1) SOH PREDICTION RESULTS AND DISCUSSIONS

To verify the robustness and accuracy of the proposed method, the data of CS2_35 and CS2_37 batteries in the CALCE dataset are selected for the experiments. In this paper, three scenarios with different training data are applied. First, 30% of the dataset is used to train, and the other 70% is used to validate the prediction of the methods. In the following scenario, half of the data is for training, and the rest is for validation. Finally, the data used for training is 60%, and the remaining is for validation. The capacity prediction is shown in Figure 12.

The comparison between the proposed method and other methods, BiLSTM, RNN-AM, and GRU, with different training data rates using the CS2_35 dataset, is shown in the first three figures. In Figure 12a, where 30% of the dataset is used to train, it can be seen that the proposed method has the highest accuracy and the closest compared to the remaining methods. Regarding the compared models, their accuracy varies depending on different scenarios. For instance, with only 30% of the data trained, the BiLSTM model yields the closest results among the standard models. However, with an increased proportion of training data to 50%, the GRU model emerges as the superior performer, or in scenarios where 60% of the data is utilized, the RNN-AM model excels. This relates to the unstable of these models in SOH prediction. Besides, it can be seen that the models in the second and third scenarios are more accurate than the models with 30% of the training data. Likewise, when applying the CS2_37 dataset, similar results can be obtained. The proposed method has the best performance, while others show their limit in prediction ability, which can be seen in Figure 12d, Figure 12e, and Figure 12f. Besides, in some cycles, the predictions of those methods in the model with 50% training data are worse than those in the one with 30% training data. However, overall, the SOH prediction results of the standard models are also acceptable for the second and third cases. The proposed model, on the other hand, can



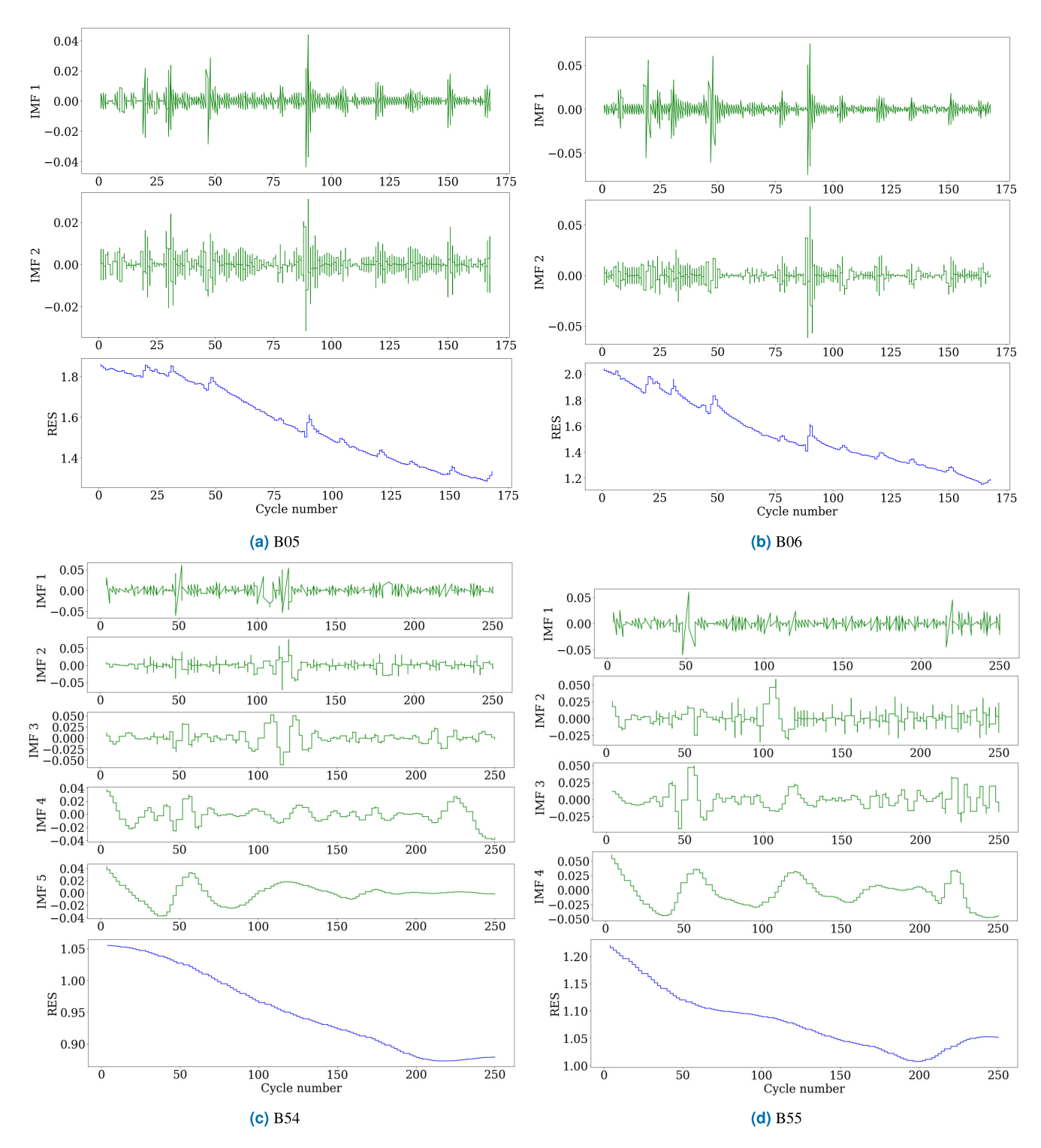


FIGURE 11. IMFs and RES data of NASA datasets.

ensure accuracy even when only 30% of the data is used for training.

2) RUL PREDICTION RESULTS AND DISCUSSIONS The RUL prediction results are shown in Table 3. It should be noted that the start point in each model can be calculated

based on the proportion of training data. Analyzing the data shows that the predicted RUL of the proposed method is closest to the real RUL of the datasets when 30%,50%, or 60% of the total data are used to train, respectively. For the dataset of the CS2_35 battery, in the first scenario, while the real RUL is 419 cycles, the predicted RUL of the hybrid

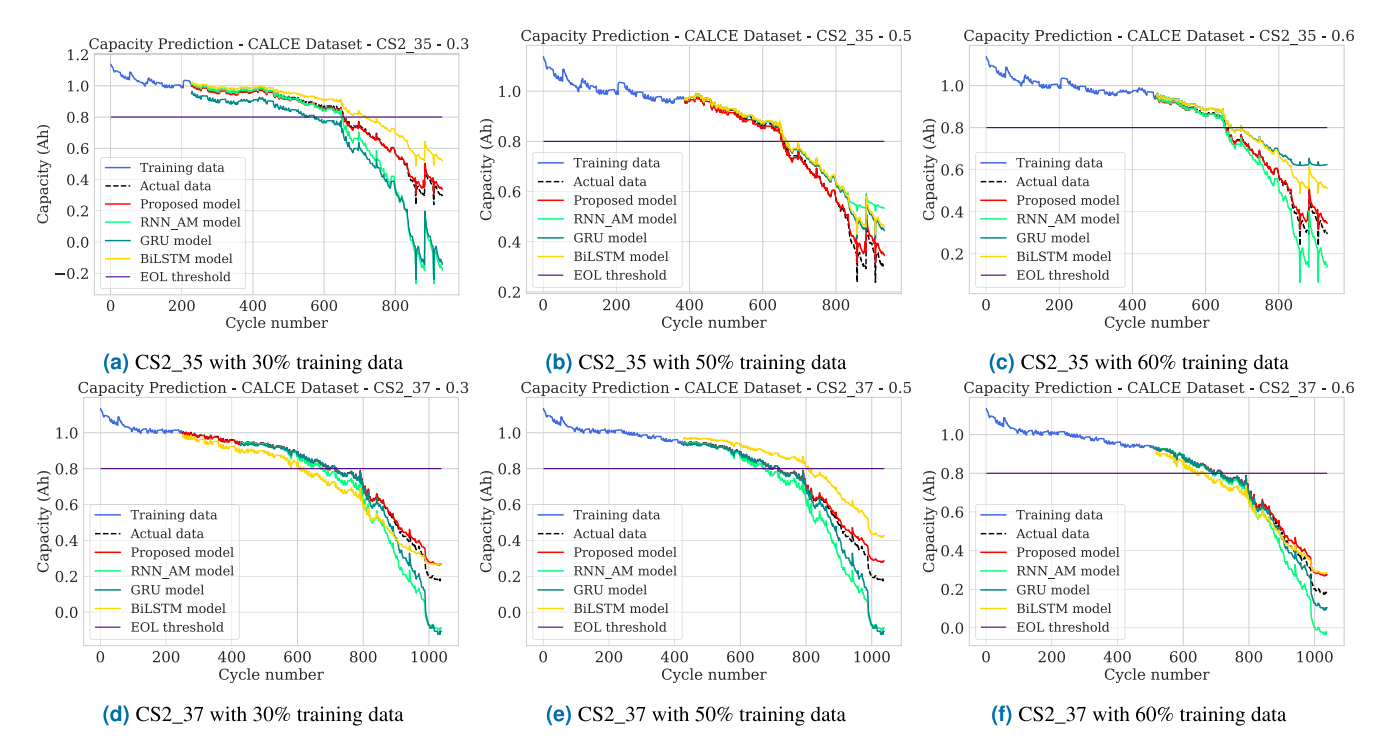


FIGURE 12. The capacity prediction of CS2_35 and CS2_37.

model is 426 cycles, and RE is just 0.017, compared to 0.0181 when applying the BiLSTM method. Or when 60% of the data is used to train, the prediction RUL of the technique in this paper is equal to 184 cycles, the actual RUL of the dataset. In the CS2_37 battery, the difference between the predicted RUL of the proposed method and the real RUL is just six cycles in the 30%-training-data case, and there are no differences between them in the other cases. However, other methods recorded significant AE, which demonstrated the instability of those methods. For instance, the RE of RNN-AM is 0.097 when the training data is 30% of the total data, but it rises to 0.131 and 0.124 when the percentage of the training data increases to 50% and 60%, respectively. Other models have also observed the same scenarios, which can be seen in Figure 12 and Table 3. From that point of view, all the models but the proposed method are unstable when predicting the SOH and RUL of the battery.

To be more reliable, the parameters in Table 3 also show that the errors RMSE and MAE of the proposed method are smaller than those of the other methods. When 60% of the data is used to train when applying CS2_35 battery, RMSE, and MAE of the proposed method are 0.014 and 0.012, which reduce at least 71% and 66% compared to other algorithms, respectively. Similar results can also be obtained in the CS2_37 dataset. In all cases, the RMSE and MAE of the proposed method decreased by at least 48% and 19% compared to those of other methods, respectively. From those results, when using 50% or 60% of the dataset's data to train, the errors of the compared model can be accepted, while the proposed model demonstrates forecasting ability even when

using only 30% of the data for training, provided prediction results close to the actual degradation data. Remarkably, the RMSE, MAE, and AE of this model in the 30% scenario are even lower than those of some models with a higher training percentage.

D. NASA BATTERY DATASET

1) SOH PREDICTION AND DISCUSSIONS

When using the NASA dataset, the SOH prediction and validation are implemented similarly to the CALCE dataset. The performance of the proposed method is compared with other techniques in each scenario: 30%, 50%, and 60% of training data when applying the data of B05, B06, B54, and B55 batteries, respectively. Figure 13 and Figure 14 show that the proposed method predicts the capacity curves closest to the actual capacity curve in all cases and both battery datasets. Although the batteries in the NASA dataset have fewer data points expressed by the number of cycles compared to CALCE data, the proposed model can still give accurate degradation curves. In B05, since the training data is 60%, BiLSTM, RNN-AM, and GRU capacity curves do not follow strictly the real one. The BiLSTM model shows the worst prediction in most cases in each battery dataset, especially in the B05 and B06 datasets. There is a considerable deviation between the BiLSTM's prediction curve and other models and the actual data. Besides, the instability of those models can be expressed by observing the

In some cases, the capacity curves of the compared models are above the real ones, while in the remaining cases,



TABLE 3. RUL prediction and errors validation of CS2_35 and CS2_37.

Battery	Starting Point	Algorithms	RUL_{re}	RUL_{pr}	AE	RE	RMSE	MAE
		BiLSTM		495	76	0.181	0.090	0.064
	227	RNN-AM	419	409	10	0.024	0.125	0.059
	22,	GRU	117	339	80	0.191	0.144	0.042
		Proposed model		426	7	0.017	0.031	0.017
		BiLSTM		286	24	0.092	0.066	0.052
CS2_35	387	RNN-AM	262	257	5	0.019	0.074	0.042
	307	GRU		286	24	0.092	0.064	0.048
		Proposed model		263	1	0.004	0.015	0.012
	466	BiLSTM	184	191	7	0.038	0.057	0.039
		RNN-AM		179	5	0.027	0.049	0.029
		GRU		200	16	0.087	0.101	0.064
		Proposed model		184	0	0	0.014	0.010
	250	BiLSTM	454	556	102	0.225	0.071	0.058
		RNN-AM		410	44	0.097	0.114	0.061
		GRU		417	37	0.081	0.096	0.045
		Proposed model		460	6	0.013	0.033	0.022
	426	BiLSTM	283	356	73	0.258	0.046	0.028
CS2_37		RNN-AM		246	37	0.131	0.062	0.026
		GRU		281	2	0.007	0.062	0.046
		Proposed model		283	0	0	0.024	0.011
	517	BiLSTM	194	206	12	0.062	0.039	0.021
		RNN-AM		170	24	0.124	0.059	0.033
		GRU		189	5	0.026	0.019	0.011
		Proposed model		194	0	0	0.019	0.009

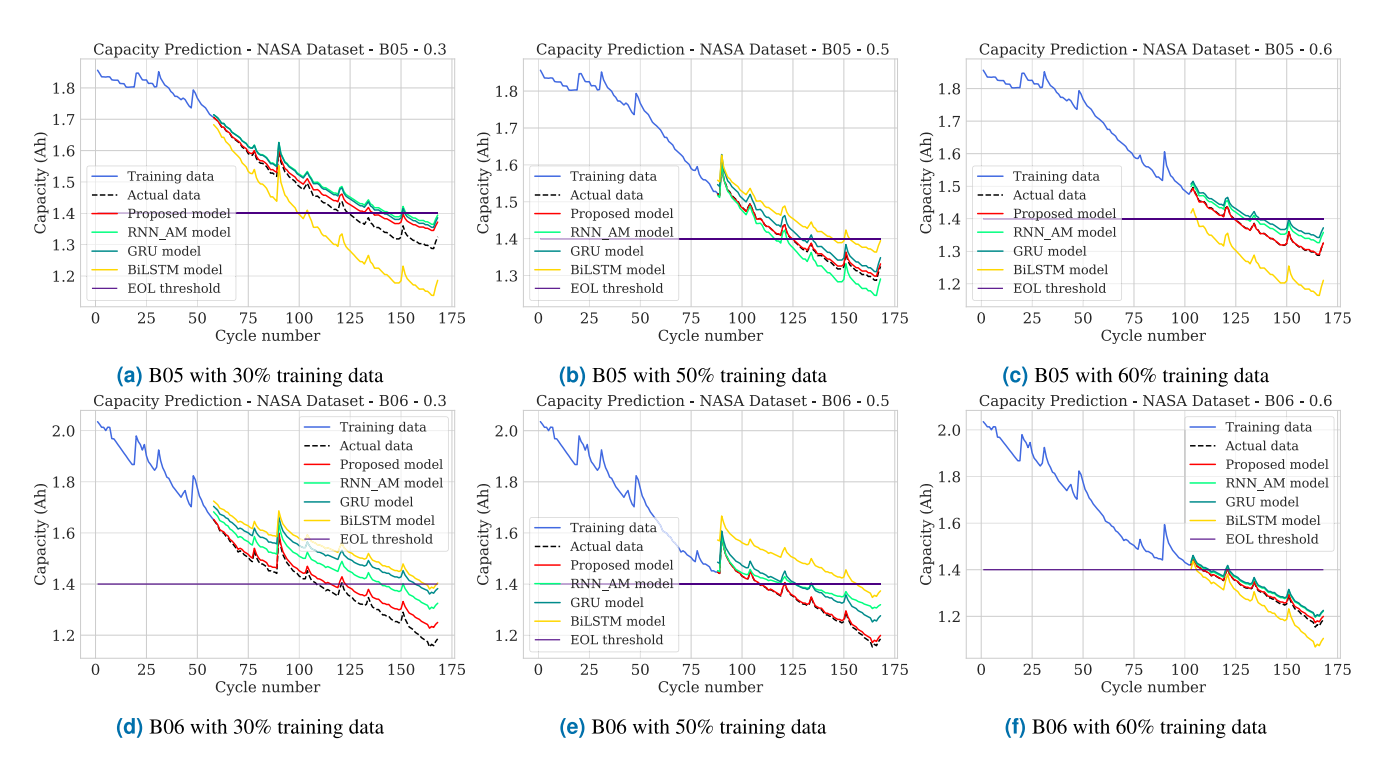


FIGURE 13. The capacity prediction of B05 and B06.

the models show the SOH predictions lower than the data used. When the proportion of the data training increases from 30% to 60%, the SOH prediction curves of the four

models become more and more accurate. Moreover, in some cases, the starting point of the compared models can not catch the endpoint of the data used to train. This issue



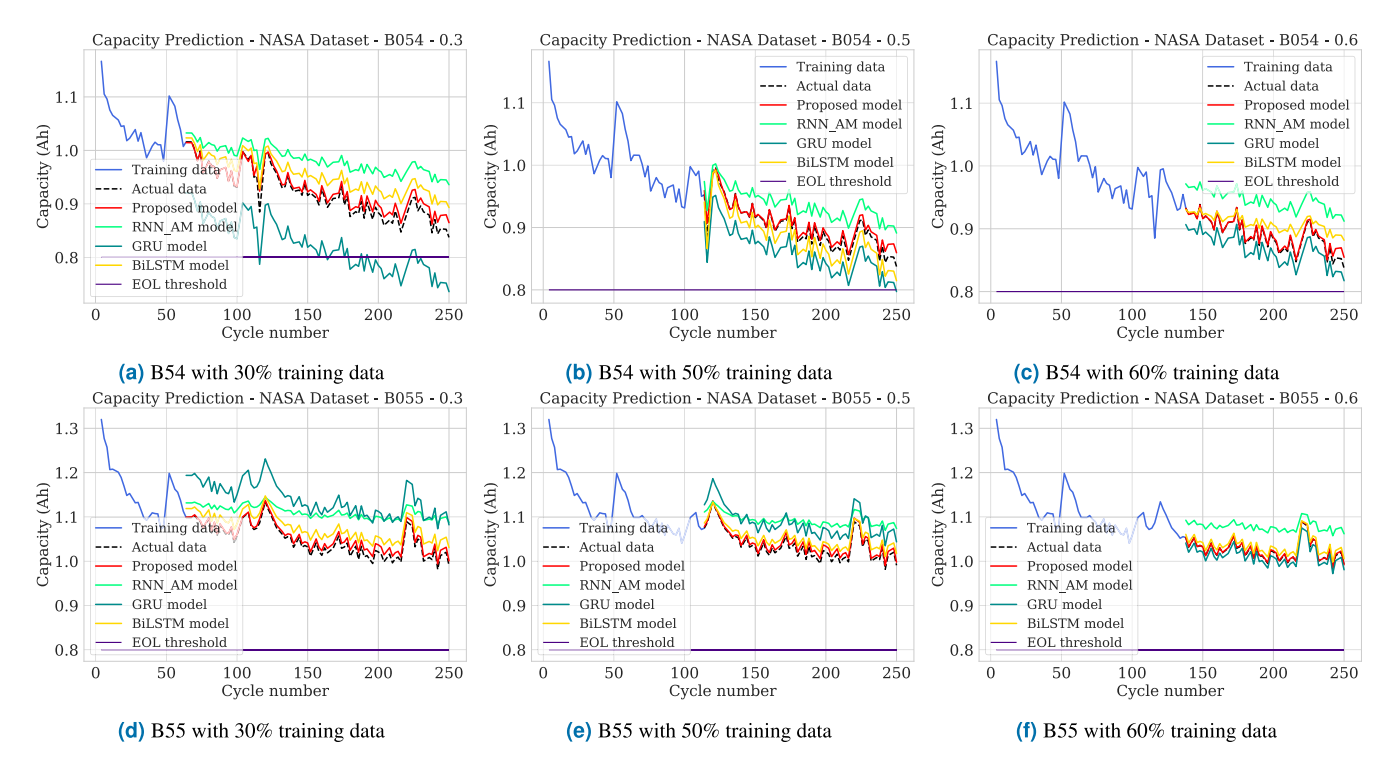


FIGURE 14. The capacity prediction of B54 and B55.

TABLE 4. RUL prediction and errors validation of B05 and B06.

Battery	Starting Point	Algorithms	RUL_{re}	RUL_{pr}	AE	RE	RMSE	MAE
		BiLSTM		41	25	0.379	0.103	0.096
	58	RNN-AM	66	0	66	1.000	0.091	0.088
		GRU	00	30	36	0.545	0.152	0.467
		Proposed model		78	12	0.182	0.030	0.024
		BiLSTM		60	24	0.667	0.058	0.057
B05	88	RNN-AM	36	27	21	0.583	0.024	0.022
		GRU	30	40	3	0.083	0.024	0.024
		Proposed model		36	0	0	0.005	0.004
		BiLSTM	21	2	19	0.905	0.102	0.101
	103	RNN-AM		15	6	0.285	0.018	0.017
		GRU		24	3	0.143	0.021	0.018
		Proposed model		22	1	0.045	0.002	0.001
	58	BiLSTM	50	103	53	1.060	0.162	0.101
		RNN-AM		105	55	1.100	0.172	0.168
		GRU		0	105	2.100	0.208	0.206
		Proposed model		57	7	0.140	0.034	0.029
	88	BiLSTM	20	68	48	2.400	0.155	0.153
B06		RNN-AM		17	3	0.150	0.037	0.032
		GRU		37	17	0.850	0.047	0.048
		Proposed model		20	0	0	0.006	0.005
	103	BiLSTM	5	2	3	0.600	0.055	0.051
		GNN-AM		2	3	0.600	0.037	0.034
		GRU		13	8	1.600	0.036	0.035
		Proposed model		0	0	0	0.007	0.005

occurs mainly in the benchmark models in most batteries with all three scenarios. In general, the proposed method

shows the best performance among all four models in all cases.



TABLE 5. RUL prediction and errors validation of B54 and B55.

Scenario	Algorithms	B5	i 4	B55		
Scenario	Aigoriums	RMSE	MAE	RMSE	MAE	
	BiLSTM	0.034	0.032	0.030	0.029	
30%	RNN-AM	0.064	0.061	0.066	0.063	
2070	GRU	0.097	0.097	0.093	0.093	
	Proposed model	0.012	0.009	0.010	0.008	
	BiLSTM	0.018	0.018	0.019	0.018	
50%	RNN-AM	0.037	0.035	0.061	0.058	
	GRU	0.042	0.041	0.052	0.052	
	Proposed model	0	0	0.007	0.008	
60%	BiLSTM	0.030	0.029	0.011	0.011	
	RNN-AM	0.055	0.054	0.055	0.054	
	GRU	0.024	0.023	0.011	0.010	
	Proposed model	0	0	0.003	0.002	

2) RUL PREDICTION AND DISCUSSION

The RUL prediction results are shown in Table 4 and Table 5. It is noted that there are no RUL prediction results for B54 and B55 batteries. The reason is that the SOHs of those batteries do not reach the EOL, which can be seen in Figure 14. Analyzing the data shows that the predicted RUL of the proposed method is closest to the real RUL of the datasets when 30%, 50%, or 60% of the total data are used to train, respectively. For the dataset of the B05 battery, in the model with 30% training data, while the real RUL is 66 cycles, the RUL that the proposed method predicted is 78 cycles, and RE is just 0.182, compared to 0.545, 1.000, and 0.379 when applying GRU, RNN-AM, and BiLSTM methods, respectively. In addition, when 60% of the data is used to train, the prediction RUL of the method in this paper is equal to 22 cycles, with only one deviation from the real RUL. In the B06 battery, the difference between the predicted RUL of the proposed method and the real RUL is just seven cycles in the 30%-training-data case, and there are no differences between them in the other cases. It can be seen that when the proportion of the data used to learn increases, the accuracy in predicting the RUL is also improved. Additionally, the RE in each scenario of B05 and B06 batteries decreases when applying different models and analyzing the start point. Other methods show their worse forecasting ability where their AE and RE are mainly greater than the proposed method, especially the BiLSTM method, which has the worst prediction about RUL.

Furthermore, the parameters in Table 4 and Table 5 also show that the errors RMSE and MAE of the proposed method are smaller than those of the other methods. When considering the dataset of the B05 battery, RMSE and MAE of the proposed method reduce at least 67% and 73% compared to other algorithms, respectively. The same scenarios occur when considering batteries B54 and B55 with different degradation data. The proposed model performs a better forecasting ability compared to other models, especially in the case of using 30% of the total data to train where the RMSE and MAE of the proposed method reduce at least 65% and 72% for B54, or at least 67% and 72% for B55, respectively. Moreover, in some cases, the predicted model

has zero errors, which indicates the absolute accuracy in SOH prediction. In short, the proposed method, including EMD, CNN, BiLSTM, and AM models, can further promote SOH and RUL prediction accuracy.

V. CONCLUSION

Predicting accurately the SOH and RUL is essential to ensure the reliability, safety, and maintenance of the Li-ion battery system. In this paper, an innovative method combined with EMD, CNN, BiLSTM, and AM is proposed to predict the SOH and RUL of the battery. First, the HIs are extracted and validated for their correlation with the SOH. Then, the EMD method is used to extract the capacity as well as HI data from the dataset into several IMF sequences and a residual sequence, and they are used as input parameters. Based on the actual degradation capacity data of the battery and input parameters, the proposed method will bring out its SOH and RUL predictions. This research selects two types of datasets, CALCE and NASA, with different training and testing data ratios to show how they affect the prediction results. Three other methods, BiLSTM, RNN-AM, and GRU, are compared with the proposed method to verify this method. The results demonstrate that the proposed method is the most accurate and robust in predicting the SOH and RUL of the battery. When considering the SOH prediction of the CALCE datasets, the RMSE and MAE of the proposed method decrease by at least 48% and 19% compared to other methods. A similar scenario occurs when using the NASA battery datasets, where the errors, including AE, RE, RMSE, and MAE, are also the smallest values when applying this work's method. In this work, however, the number of IMF extracted using the EMD model in the pre-processing step is not objectively determined. Therefore, it would be necessary to find a suitable function or procedure showing the relationship between the complexity of the data and the number of IMF extracted. The application of the proposed model to a larger-scale system and considering other battery datasets will also be further considered.

REFERENCES

- X. Hu, F. Feng, K. Liu, L. Zhang, J. Xie, and B. Liu, "State estimation for advanced battery management: Key challenges and future trends," *Renew. Sustain. Energy Rev.*, vol. 114, Oct. 2019, Art. no. 109334.
- [2] B. Smith, "Chevrolet volt battery incident-NHTSA summary report," Accident Reconstruction J., vol. 23, no. 5, pp. 31–37, 2013.
- [3] K. S. Ng, C.-S. Moo, Y.-P. Chen, and Y.-C. Hsieh, "Enhanced Coulomb counting method for estimating state-of-charge and state-of-health of lithium-ion batteries," *Appl. Energy*, vol. 86, no. 9, pp. 1506–1511, Sep. 2009.
- [4] I. Babaeiyazdi, A. Rezaei-Zare, and S. Shokrzadeh, "State of charge prediction of EV Li-ion batteries using EIS: A machine learning approach," *Energy*, vol. 223, May 2021, Art. no. 120116.
- [5] P. Ren, S. Wang, M. He, and W. Cao, "Novel strategy based on improved Kalman filter algorithm for state of health evaluation of hybrid electric vehicles Li-ion batteries during short- and longer term operating conditions," *J. Power Electron.*, vol. 21, no. 8, pp. 1190–1199, May 2021.
- [6] L. Ling and Y. Wei, "State-of-charge and state-of-health estimation for lithium-ion batteries based on dual fractional-order extended Kalman filter and online parameter identification," *IEEE Access*, vol. 9, pp. 47588–47602, 2021.



- [7] J. Li, M. Ye, K. Gao, X. Xu, M. Wei, and S. Jiao, "Joint estimation of state of charge and state of health for lithium-ion battery based on dual adaptive extended Kalman filter," *Int. J. Energy Res.*, vol. 45, no. 9, pp. 13307–13322, 2021.
- [8] T. Wu, S. Liu, Z. Wang, and Y. Huang, "SOC and SOH joint estimation of lithium-ion battery based on improved particle filter algorithm," *J. Electr. Eng. Technol.*, vol. 17, no. 1, pp. 307–317, Jan. 2022.
- [9] K. A. Severson, P. M. Attia, N. Jin, N. Perkins, B. Jiang, Z. Yang, M. H. Chen, M. Aykol, P. K. Herring, D. Fraggedakis, M. Z. Bazant, S. J. Harris, W. C. Chueh, and R. D. Braatz, "Data-driven prediction of battery cycle life before capacity degradation," *Nature Energy*, vol. 4, no. 5, pp. 383–391, Mar. 2019.
- [10] D. Yang, Y. Wang, R. Pan, R. Chen, and Z. Chen, "A neural network based state-of-health estimation of lithium-ion battery in electric vehicles," *Energy Proc.*, vol. 105, pp. 2059–2064, May 2017.
- [11] Y. Ma, C. Shan, J. Gao, and H. Chen, "A novel method for state of health estimation of lithium-ion batteries based on improved LSTM and health indicators extraction," *Energy*, vol. 251, Jul. 2022, Art. no. 123973.
- [12] J. Jia, J. Liang, Y. Shi, J. Wen, X. Pang, and J. Zeng, "SOH and RUL prediction of lithium-ion batteries based on Gaussian process regression with indirect health indicators," *Energies*, vol. 13, no. 2, p. 375, Jan. 2020.
- [13] S. B. Vilsen and D.-I. Stroe, "Battery state-of-health modelling by multiple linear regression," *J. Cleaner Prod.*, vol. 290, Mar. 2021, Art. no. 125700.
- [14] M. Lin, D. Wu, J. Meng, J. Wu, and H. Wu, "A multi-feature-based multi-model fusion method for state of health estimation of lithium-ion batteries," *J. Power Sources*, vol. 518, Jan. 2022, Art. no. 230774.
- [15] J. Lu, R. Xiong, J. Tian, C. Wang, C.-W. Hsu, N.-T. Tsou, F. Sun, and J. Li, "Battery degradation prediction against uncertain future conditions with recurrent neural network enabled deep learning," *Energy Storage Mater.*, vol. 50, pp. 139–151, Sep. 2022.
- [16] L. Zhang, B. Wang, X. Yuan, and P. Liang, "Remaining useful life prediction via improved CNN, GRU and residual attention mechanism with soft thresholding," *IEEE Sensors J.*, vol. 22, no. 15, pp. 15178–15190, Aug. 2022.
- [17] L. Ren, J. Dong, X. Wang, Z. Meng, L. Zhao, and M. J. Deen, "A data-driven Auto-CNN-LSTM prediction model for lithium-ion battery remaining useful life," *IEEE Trans. Ind. Informat.*, vol. 17, no. 5, pp. 3478–3487, May 2021.
- [18] L. Ungurean, M. V. Micea, and G. Cârstoiu, "Online state of health prediction method for lithium-ion batteries, based on gated recurrent unit neural networks," *Int. J. Energy Res.*, vol. 44, no. 8, pp. 6767–6777, Jun. 2020.
- [19] Y. Li, L. Luo, C. Zhang, and H. Liu, "State of health assessment for lithium-ion batteries using incremental energy analysis and bidirectional long short-term memory," World Electric Vehicle J., vol. 14, no. 7, p. 188, Jul. 2023.
- [20] J. Lin, J. Ma, J. Zhu, and Y. Cui, "Short-term load forecasting based on LSTM networks considering attention mechanism," *Int. J. Electr. Power Energy Syst.*, vol. 137, May 2022, Art. no. 107818.
- [21] Y. Cai, G. Xu, D. Yang, H. Tian, F. Zhou, and J. Guo, "On-line multi-gas component measurement in the mud logging process based on Raman spectroscopy combined with a CNN-LSTM-AM hybrid model," *Analytica Chim. Acta*, vol. 1259, Jun. 2023, Art. no. 341200.
- [22] F.-K. Wang, Z. E. Amogne, J.-H. Chou, and C. Tseng, "Online remaining useful life prediction of lithium-ion batteries using bidirectional long shortterm memory with attention mechanism," *Energy*, vol. 254, Sep. 2022, Art. no. 124344.
- [23] X. Gu, K. W. See, P. Li, K. Shan, Y. Wang, L. Zhao, K. C. Lim, and N. Zhang, "A novel state-of-health estimation for the lithium-ion battery using a convolutional neural network and transformer model," *Energy*, vol. 262, Jan. 2023, Art. no. 125501.
- [24] G. Cheng, X. Wang, and Y. He, "Remaining useful life and state of health prediction for lithium batteries based on empirical mode decomposition and a long and short memory neural network," *Energy*, vol. 232, Oct. 2021, Art. no. 121022.
- [25] J. C. Chen, T.-L. Chen, W.-J. Liu, C. C. Cheng, and M.-G. Li, "Combining empirical mode decomposition and deep recurrent neural networks for predictive maintenance of lithium-ion battery," *Adv. Eng. Informat.*, vol. 50, Oct. 2021, Art. no. 101405.
- [26] L. Le Thi Minh, A. Vu Quoc, T. N. Duc, and G. Fujita, "Forecasting state-of-health of battery based on combined EMD-CNN-BiLSTM-SM method," in *Proc. Asia Meeting Environ. Electr. Eng. (EEE-AM)*, Nov. 2023, pp. 1–5.

- [27] W. Zhou, Q. Lu, and Y. Zheng, "Review on the selection of health indicator for lithium ion batteries," *Machines*, vol. 10, no. 7, p. 512, Jun. 2022.
- [28] X. Wang, B. Hu, X. Su, L. Xu, and D. Zhu, "State of health estimation for lithium-ion batteries using random forest and gated recurrent unit," *J. Energy Storage*, vol. 76, Jan. 2024, Art. no. 109796.
- [29] S. Liu, Z. Chen, L. Yuan, Z. Xu, L. Jin, and C. Zhang, "State of health estimation of lithium-ion batteries based on multi-feature extraction and temporal convolutional network," *J. Energy Storage*, vol. 75, Jan. 2024, Art. no. 109658.
- [30] K. Asakura, M. Shimomura, and T. Shodai, "Study of life evaluation methods for Li-ion batteries for backup applications," *J. Power Sources*, vols. 119–121, pp. 902–905, Jun. 2003.
- [31] Calce Battery Data. Center of Advanced Life Cycle Engineering. Accessed: Jun. 12, 2023. [Online]. Available: https://web.calce.umd.edu/batteries/data.htm
- [32] Battery Data Set, NASA Prognostics Data Repository, NASA Ames Res. Center, Moffett Field, CA, USA, 2007.
- [33] X. Pang, R. Huang, J. Wen, Y. Shi, J. Jia, and J. Zeng, "A lithiumion battery RUL prediction method considering the capacity regeneration phenomenon," *Energies*, vol. 12, no. 12, p. 2247, Jun. 2019.
- [34] W. J. Conover, *Practical Nonparametric Statistics*, vol. 350. Hoboken, NJ, USA: Wiley, 1999.
- [35] N. E. Huang, Z. Shen, S. R. Long, M. C. Wu, H. H. Shih, Q. Zheng, N.-C. Yen, C. C. Tung, and H. H. Liu, "The empirical mode decomposition and the Hilbert spectrum for nonlinear and non-stationary time series analysis," *Proc. Roy. Soc. London Ser. A, Math., Phys. Eng. Sci.*, vol. 454, pp. 903–995, Mar. 1998.
- [36] K. Liu, Y. Shang, Q. Ouyang, and W. D. Widanage, "A data-driven approach with uncertainty quantification for predicting future capacities and remaining useful life of lithium-ion battery," *IEEE Trans. Ind. Electron.*, vol. 68, no. 4, pp. 3170–3180, Apr. 2021.
- [37] J. Gu, Z. Wang, J. Kuen, L. Ma, A. Shahroudy, B. Shuai, T. Liu, X. Wang, G. Wang, and J. Cai, "Recent advances in convolutional neural networks," *Pattern Recognition*, vol. 77, pp. 354–377, May 2018.
- [38] K. Fukushima, "Neocognitron: A self-organizing neural network model for a mechanism of pattern recognition unaffected by shift in position," *Biol. Cybern.*, vol. 36, no. 4, pp. 193–202, Apr. 1980.
- [39] Y. LeCun, B. Boser, J. Denker, D. Henderson, R. Howard, W. Hubbard, and L. Jackel, "Handwritten digit recognition with a back-propagation network," in *Advances in Neural Information Processing Systems*, vol. 2, D. Touretzky, Ed., Burlington, MA, USA: Morgan-Kaufmann, 1989. [Online]. Available: https://proceedings.neurips.cc/paper_files/paper/1989/file/53c3bce66e43be4f209556518c2fcb54-Paper.pdf
- [40] R. Sánchez-Reolid, F. López de la Rosa, M. T. López, and A. Fernández-Caballero, "One-dimensional convolutional neural networks for low/high arousal classification from electrodermal activity," *Biomed. Signal Process. Control*, vol. 71, Jan. 2022, Art. no. 103203.
- [41] S. Hochreiter and J. Schmidhuber, "Long short-term memory," *Neural Comput.*, vol. 9, no. 8, pp. 1735–1780, Nov. 1997.
- [42] N. D. Tuyen, L. V. Thinh, V. X. S. Huu, and G. Fujita, "Forecasting I-V characteristic of PV modules considering real operating conditions using numerical method and deep learning," in *Proc. Int. Conf. Smart Grids Energy Syst. (SGES)*, Nov. 2020, pp. 544–549.
- [43] Z. Niu, G. Zhong, and H. Yu, "A review on the attention mechanism of deep learning," *Neurocomputing*, vol. 452, pp. 48–62, May 2021.
- [44] L. Xiang, P. Wang, X. Yang, A. Hu, and H. Su, "Fault detection of wind turbine based on SCADA data analysis using CNN and LSTM with attention mechanism," *Measurement*, vol. 175, Apr. 2021, Art. no. 109094.



LE THI MINH LIEN is currently pursuing the Electrical Engineering degree in electrical technique with the School of Electrical and Electronic Engineering, Hanoi University of Science and Technology. She is a Research Assistant with the 100% Renewable Energy Laboratory, Hanoi University of Science and Technology, under the supervision of Assoc. Prof. Nguyen Duc Tuyen. Her research interests include determining the optimal BESS sizing and placement in the

distribution grid and estimating the SOH and RUL of the battery.





VU QUOC ANH is currently a Junior with the School of Electrical and Electronic Engineering, Hanoi University of Science and Technology, specializing in power systems and renewable energy. He is also a Research Assistant with the 100% Renewable Energy Laboratory, Hanoi University of Science and Technology, under the supervision of Assoc. Prof. Nguyen Duc Tuyen. His academic pursuits revolve around exploring optimal BESS sizing within the distribution grid

and assessing the SOH and RUL of batteries.



GORO FUJITA (Member, IEEE) received the B.E., M.E., and Ph.D. degrees in electrical engineering from Hosei University, Tokyo, Japan, in 1992, 1994, and 1997, respectively. He is currently a Professor with Shibaura Institute of Technology, Japan. His research interest includes power system control. He is a member of the IEE of Japan.

. . .



NGUYEN DUC TUYEN (Senior Member, IEEE) received the bachelor's degree in electrical engineering from Hanoi University of Science and Technology, in 2006, and the master's and Ph.D. degrees from Shibaura Institute of Technology, Tokyo, Japan, in 2009 and 2012, respectively. He was an Associate Professor with Hanoi University of Science and Technology, in 2024. From 2012 to 2015, he was a Researcher with Shibaura Institute of Technology, Tokyo, and a

part-time Lecturer with Chiba University and Tokyo Wildlife College, Japan. From 2015 to 2017, he was with Tokyo University of Science, Japan. From 2017 to 2018, he conducted research at the National Institute of Industrial Science and Technology, Japan. Since 2018, he has been a Lecturer with the Department of Power Systems, Electrical Engineering School, Hanoi University of Science and Technology. He has published more than 120 journals and conference papers. He is an Active Reviewer of IET, MDPI, IEEJ, Springer, and Elsevier. He has been reviewing hundreds of papers, since 2009.